J. Astrophys. Astr. (2008) **29,** 3–16

Keynote Address: Outstanding Problems in Solar Physics

Markus J. Aschwanden
Lockheed Martin Advanced Technology Center, Solar and Astrophysics Laboratory, Bldg. 252, Org. ADBS, 3251 Hanover St., Palo Alto, CA 94304, USA.
e-mail: aschwanden@lmsal.com

Abstract. Celebrating the diamond jubilee of the Physics Research Laboratory (PRL) in Ahmedabad, India, we look back over the last six decades in solar physics and contemplate on the ten outstanding problems (or research foci) in solar physics:

1. The solar neutrino problem
2. Structure of the solar interior (helioseismology)
3. The solar magnetic field (dynamo, solar cycle, corona)
4. Hydrodynamics of coronal loops
5. MHD oscillations and waves (coronal seismology)
6. The coronal heating problem
7. Self-organized criticality (from nanoflares to giant flares)
8. Magnetic reconnection processes
9. Particle acceleration processes
10. Coronal mass ejections and coronal dimming

The first two problems have been largely solved recently, while the other eight selected problems are still pending a final solution, and thus remain persistent *Challenges for Solar Cycle 24*, the theme of this jubilee conference.

Key words. Solar neutrinos—solar interior—helioseismology—solar magnetic field—solar: corona, cycle, flares—magnetohydrodynamics (MHD)—MHD: oscillations, waves—coronal: heating, dimming—self-organized criticality—particle acceleration—coronal mass ejections (CME).

1. The solar neutrino problem

The ultimate source of energy in our Sun is the nuclear burning of hydrogen to helium, which occurs in the central region of the Sun at a temperature of 15 million degrees. This was first understood in the 1920s, when Hans Bethe, George Gamow, and Carl von Weizsäcker identified the relevant nuclear chain reactions, i.e., the proton–proton (p–p) and the carbon–nitrogen–oxygen (CNO) chain reactions. Both chain reactions of nuclear fusion of hydrogen to helium produce neutrinos, which have little interaction with matter and escape the Sun. Solar neutrinos have been detected since 1967 by Raymond Davis Jr. in a chlorine tank in the Homestake Gold Mine in South

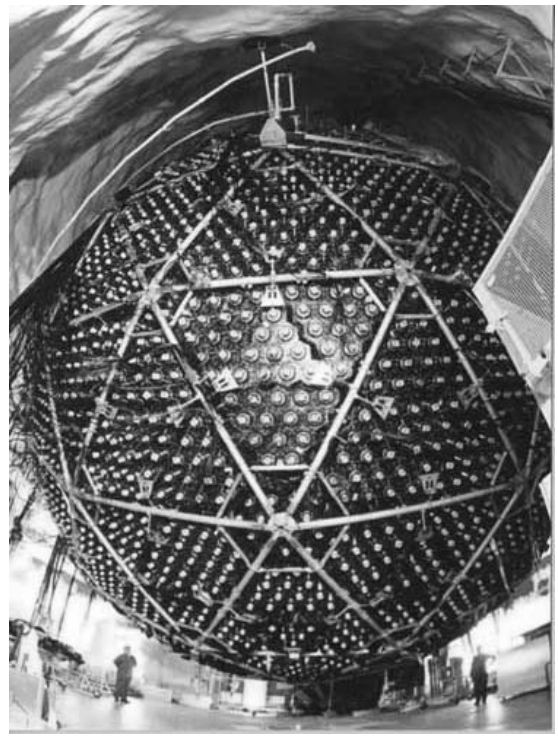

Figure 1. The Sudbury Neutrino Observatory (SNO) in Ontario, Canada, featuring a heavy-water Cherenkov detector that is designed to detect solar neutrinos. It uses 1000 tons of heavy water and 9600 photomultiplier tubes mounted on a geodesic support structure within a 30 meter barrel-shaped cavity, located in the deepest part of the Sudbury mine (Courtesy of SNO).

Dakota, but only about 1/3 of the theoretically predicted neutrino rate was detected over 35 years. This substantial discrepancy raised questions of whether the astrophysical models of the solar interior were incorrect or whether we missed some fundamental part of nuclear physics, which constituted a "power struggle" between astrophysics and particle physics. More powerful particle detectors came online, such as the gallium detector *GALLEX* in Italy and *SAGE* in Russia, sensitive to electronic neutrinos ν_e, as produced by the main nuclear process $4p \mapsto {}^4\mathrm{He} + 2\mathrm{e}^+ + 2\nu_e$. However, Pontecorvo and Gribov predicted already in 1969 that low-energy solar neutrinos undergo a *personality disorder* on their travel to earth and oscillate into other flavors of muonic (ν_μ) and tauonic neutrinos (ν_τ), which turned out to be the solution of the *missing neutrino problem*. The first generation of detectors was only sensitive to the highest-energy (electronic) neutrinos, such as the chlorine tank of Raymond Davis Jr, while the *Kamiokande* and *Super-Kamiokande-I* pure-water experiments and the *Sudbury Neutrino Observatory* (*SNO*, Ontario, Canada; Fig. 1) heavy-water experiments are also somewhat sensitive to the muonic and tauonic neutrinos. So it was the *SNO* that measured for the first time all three lepton flavors (Ahmad *et al.* 2002), which brilliantly confirmed the theory of *neutrino (flavor) oscillations*, and this way also corroborated the astrophysical model and the chemical composition of the solar interior to be

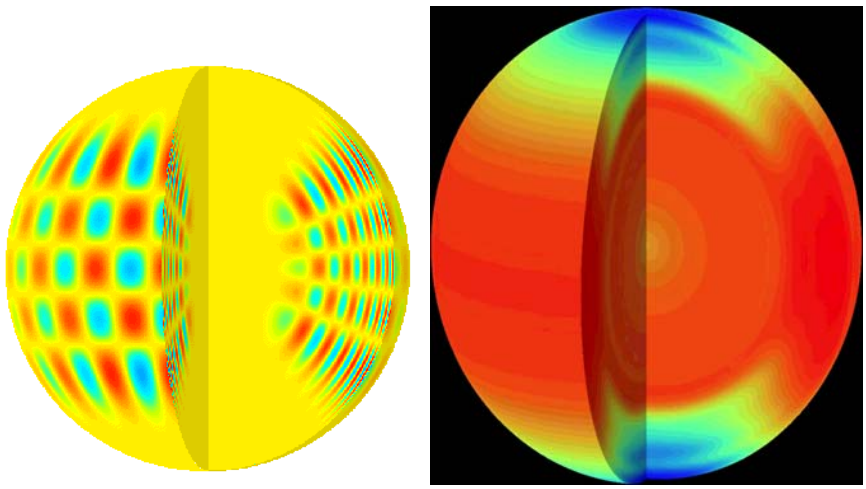

Figure 2. Left: A global acoustic p-mode wave is visualized: The radial order is $n = 14$, the angular degree is $l = 20$, the angular order is $m = 16$, and the frequency is $\nu = 2935.88 \pm 0.1\ \mu$Hz, observed with SoHO/MDI (Michelson Doppler Imager). **Right:** The internal rotation rate is shown with a greyscale, measured with SoHO/MDI during May 1996–April 1997. The fastest rotation rate ($P \approx 25$ days) is rendered with a black color, while the slowest rate ($P \approx 35$ days) is given with white color. Note that the rotation rate is rigid in the interior radiative zone, while it is differential in the outer convection zone (Courtesy of SoHO/MDI Team and NASA).

correct (Bellerive 2004; Bahcall 2005). Raymond Davis Jr. garnered the Nobel Price in Physics 2002 for his pioneering work in neutrino observations (Davis 2003), while the uncrowned John Bahcall, who accomplished most of the fundamental theoretical work around the solar neutrino problem, deceased in 2005.

2. The structure of the solar interior

On one side, the internal structure of the Sun has been inferred from theoretical models: either with hydrostatic equilibrium models, or with time-dependent numerical simulations of the Sun's lifetime evolution. On the other side, experimental verification has been achieved with high accuracy by means of helioseismology, which was discovered in the decade of 1960–1970, from global oscillations on the solar surface in visible light. Velocity oscillations were first measured by R. Leighton, and then interpreted in 1970 as standing sound waves in the solar convection zone by R. Ulrich, C. Wolfe, and J. Leibacher. These acoustic oscillations, also called *p-modes* (pressure-driven waves), are detectable from fundamental up to harmonic numbers of ≈ 1000, and are most conspicuous in dispersion diagrams, $\omega(k)$, where each harmonic shows up as a separate ridge, when the oscillation frequency (ω) is plotted as a function of the wavelength λ. An example of a p-mode standing wave is shown in Fig. 2 (left). Since the density and temperature monotonically increase with depth inside the Sun, the sound speed varies as a function of the radial distance from Sun center. P-mode waves excited at the solar surface propagate downward and are refracted towards the surface, where the low harmonics penetrate very deep, while high harmonics are confined to the outermost

layers of the solar interior. By measuring the frequencies at each harmonic, the sound speed can be inverted as a function of the depth, and this way the density and temperature profile of the solar interior can be inferred and unknown parameters of theoretical standard models can be constrained, such as the abundance of helium and heavier elements. The detailed elemental abundance of helium and heavier elements is still a key problem of cosmological significance (e.g., Bahcall *et al.* 2005, 2006).

Exploiting the Doppler effect, frequency shifts of the p-mode oscillations can be used to measure the internal velocity rate as a function of depth and latitude, as shown in Fig. 2 (right). A layer of rapid change in the internal rotation rate was discovered this way at the bottom of the convection zone, the so-called *tachocline* (at 0.693 ± 0.002 solar radius, with a thickness of 0.039 ± 0.013 solar radius). The physical structure of the tachocline is still considered as a key to understand the solar dynamo and the generation of magnetic fields (e.g., Gilman 2000).

Besides the p-mode waves, *gravity waves* (*g-modes*) are suspected to exist in the solar core, where buoyancy rather than pressure supplies the restoring force. These gravity waves were predicted to have long periods (hours) and very small velocity amplitudes, but they have not yet been convincingly detected, which represents another open problem about the deepest core of our star (e.g., Rogers & Glatzmaier 2005).

While *global helioseismology* detects p-modes as a pattern of standing waves that encompass the entire solar surface, local deviations of the sound speed can also be detected beneath sunspots and active regions, a diagnostic that is called *local helioseismology* (for reviews see, e.g., *Solar Physics*, Vol. **192**). Near sunspots, p-modes are found to have oscillation periods in the order of 3 minutes, compared to 5 minutes in active region plages and quiet-Sun regions. So, local helioseismology allows us to probe flow patterns beneath sunspots, which yields us clues on magneto-convection and large-scale flows (e.g., meridional flows) associated with the solar dynamo in general. Disturbances of the sound speed can even be used to probe the far-side of the Sun, which enables us to make frontside predictions of active regions that emerge on the backside of the Sun.

3. The solar magnetic field

There are many problems related to the physical understanding of the solar magnetic field, subject of numerous and intense studies. The most fundamental aspect is the workings of the solar dynamo in the solar interior, which generates the magnetic field we observe on the solar surface and in the corona. The basic idea of the solar dynamo has been developed in the work of Parker, Babcock, Leighton, Deubner, and Ulrich in the years after 1955. The solar dynamo consists of a poloidal field at the beginning of the solar cycle that becomes wound up (omega effect) and twisted (alpha effect) progressively due to the differential solar rotation, and finally evolves into a highly stressed toroidal field, which then breaks up by many local reconnection events (associated with flares and coronal mass ejections), leading to the decay of the solar cycle. Although we understand the basic mechanism, we still do not understand a lot of physical aspects of the solar dynamo (e.g., Charbonneau 2005). For instance, analytical models of the dynamo produce too much twisting and thus predict shorter cycles than the observed 11 years. Meridional flows have been detected with helioseismology, slow surface flows of order $\approx 20\,\mathrm{m\ s^{-1}}$, which seem to play a critical role for the solar dynamo. Moreover, opposite magnetic helicity is observed in weak and strong field

regions, another puzzle that needs to be explained by a successful dynamo model. We do not expect that a fully analytical model will reproduce the solar dynamo, since also chaotic behavior and intermittency are expected to play a role, which make a fully deterministic model problematic.

The solar photosphere is the place where the solar magnetic field is most directly observed (by means of the Zeeman effect), but this is also the magnetically most complex region due to the subphotospheric magneto-convection, which creates the granular, mesogranular, and supergranular structures. The solar dynamo is thought to produce magnetic fibrils in the tachocline and convection zone, which buoyantly rise to the surface, become mixed by turbulent magneto-convection, and become better understood only now with numerical MHD simulations (e.g., Carlsson & Stein 1997) and impressive high-resolution observations (e.g., DePontieu *et al.* 2007).

Besides the generation of the magnetic field in the solar interior, we have also fundamental problems to model the magnetic field in the solar atmosphere and corona. Potential (source-surface) models yield a reasonable first approximation of the coronal field in most cases, but they cannot reproduce twisted field lines (filaments, magnetic flux ropes) or current sheets (important for the formation of flares and coronal mass ejections), because potential fields ignore the currents by definition. Force-free models stand on a physically more sound basis, but the simplest version (of linear force-free fields) renders oversimplified models, while more general versions (nonlinear force-free fields) require large computational efforts and are insufficiently constrained by photospheric magnetograms or magnetograph data (Schrijver *et al.* 2006). There is also the fundamental problem that any extrapolation of photospheric magnetic fields bears significant uncertainties because the lowest 500 km of the chromosphere is not force-free (Metcalf *et al.* 1995). Furthermore, most magnetic field models ignore the density and temperature of the plasma, except models computed with full MHD codes. An observational constraint that is used more and more is the tracing of coronal EUV loops, because they are assumed to trace out exactly the coronal field due to the low plasma-β parameter of the corona (Fig. 3). However, the 3D reconstruction of EUV loops is still in its infancy, but automated loop recognition algorithms and stereoscopic 3D reconstructions with the new STEREO mission are rapidly developing (e.g., Wiegelmann & Inhester 2006).

4. Hydrodynamics of coronal loops

Standard models of the solar corona assume gravitational stratification and spherical symmetry, which provides a 1D model of the average density for the dominant temperature as a function of altitude. However, the solar corona is highly inhomogeneous, structured by loops (closed field lines) and plumes (open field lines in coronal holes), and more complex transient structures, which are not necessarily in hydrostatic equilibrium. The most widely used hydrostatic model of coronal loops assumes an equilibrium between a spatially uniform heating rate and the radiative and conductive loss rates, the so-called Rosner–Tucker–Vaiana (RTV) model (Rosner *et al.* 1978). Although this model predicts a scaling law between the loop apex temperature, loop length, and pressure, that approximately corresponds to the observations of hotter soft X-ray emitting loops (Rosner *et al.* 1978), the new EUV observations of coronal loops revealed density deviations up to two orders of magnitude, super-hydrostatic density scale heights, near-isothermality along the loops, and obvious dynamical behaviors,

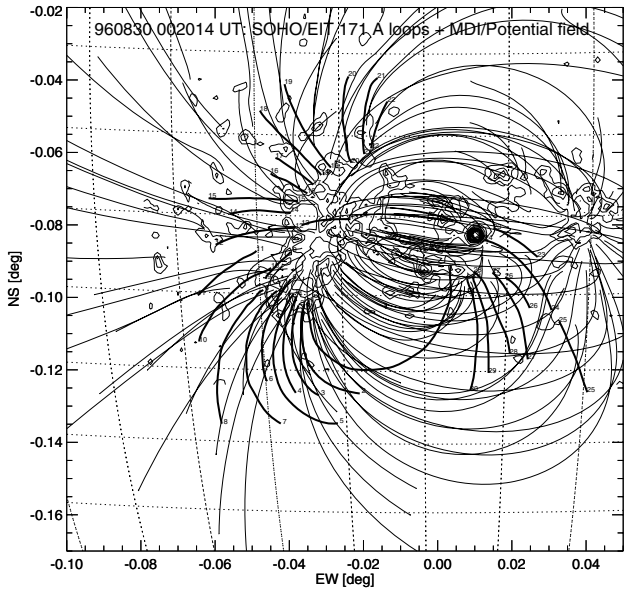

Figure 3. Magnetic field lines of an active region are shown, based on a theoretical potential field model extrapolated from magnetograms observed with SoHO/MDI on August 30, 1996 20:48 UT (thin lines), and compared with tracings of EUV loops observed simultaneously with SoHO/EIT at 171 Å (thick lines). Note the misalignment of cospatial loops and field lines, which indicates the inappropriateness of a potential field model (from Aschwanden *et al.* 1999).

properties that are all not consistent with the RTV model. We can understand that hotter soft X-ray loops agree better with the RTV model than the cooler EUV loops, because the pressure scale height in hotter loops is generally longer than the loop height, and thus the assumption of a constant pressure made in the RTV model is better fulfilled. The cooler EUV loops have a shorter density or pressure scale height, say $\lambda \approx 47{,}000$ km for 1 MK loops, and thus the gravitational stratification has to be included in hydrostatic models, which has been considered in the model of Serio *et al.* (1981).

However, the least known parameter is the spatial heating function. Serio *et al.* (1981) parameterized the heating function with an exponential heating scale height, which predicted higher loop densities and flatter temperature profiles than the RTV model, as it was actually observed in EUV loops with the TRACE spacecraft (e.g., Lenz *et al.* 1999; Aschwanden *et al.* 2000). Some active region loops were observed to have density scale heights up to four times the hydrostatic thermal scale height (Fig. 4), so they were clearly not in hydrostatic equilibrium. Although difficult to measure, plasma flows were readily detected in a number of loops, which require dynamic models, such as siphon flow models. However, what made hydrostatic models even more questionable was the observed temperature evolution, i.e., EUV loops were clearly observed most of the time to be cooling through the EUV passbands, while the hotter counterpart appeared in soft X-rays typically an hour earlier (Winebarger & Warren 2005). Generally, the observed cooling time was found to be significantly longer than the theoretically expected radiative cooling time, which required hydrodynamic models

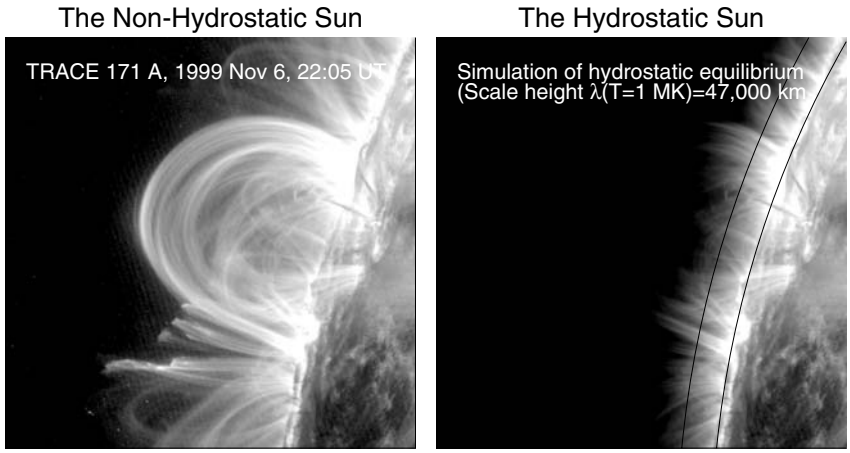

Figure 4. An active region at the limb, observed with TRACE on November 6, 1999, 22 UT, is shown on the left. These loops have a density scale height of at least four times the hydrostatic scale height (as simulated in the right panel), and thus are in a state far away from hydrostatic equilibrium (Aschwanden *et al.* 2001).

with temporally intermittent heating functions (Warren & Winebarger 2006). So, we find ourselves in abandoning hydrostatic models and delving into more complex hydrodynamic models to reconcile the observed density and temperature structure of coronal loops, not to talk about intricate data analysis problems how to separate an individual coronal loop from the complex background that contains myriads of competing other loop structures.

5. MHD oscillations and waves

Much like the discovery of helioseismology four decades ago, it was recently discovered that the solar corona contains an impressively large ensemble of plasma structures that are capable of producing sound waves and harmonic oscillations. Coronal seismology was mostly enabled by the high spatial resolution, image contrast, and time cadences of the SoHO and TRACE spacecraft in EUV images. Oscillating loops (Fig. 5), prominences, or sunspots, as well as propagating waves have been intensively studied since about 1999. While the theory of MHD oscillations was ready since about the 1980s, observational verification occurred only about two decades later. Essentially all predicted MHD wave modes have been observed and verified today, which includes MHD fast mode standing waves (kink modes and sausage modes) and MHD slow mode (acoustic) standing waves, as well as propagating MHD waves. Most of the loop oscillations occur after a filament eruption, flare, and/or coronal mass ejection (CME). It occurs that mass transport during an eruptive phenomenon causes a pressure imbalance in the surrounding coronal plasma, which displaces loops and excites this way oscillations until a new pressure equilibrium is reached. A surprising observation was also that most of these loop oscillations are strongly damped, but there is much theoretical argument about the most relevant damping mechanism. For fast MHD oscillations the two most likely damping mechanisms are phase mixing and resonant

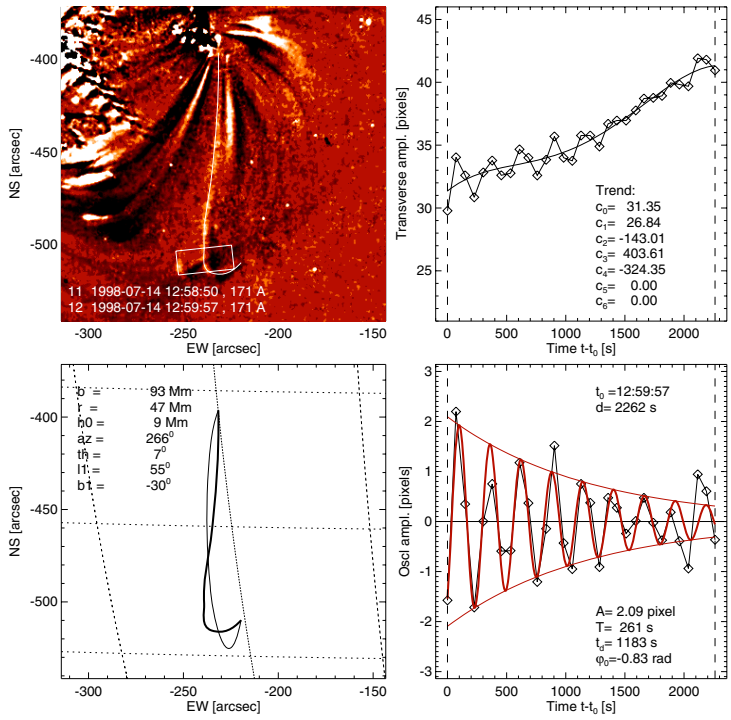

Figure 5. A loop oscillation is observed with TRACE on July 14, 1998, 13 UT: The difference image shows loop displacements with respect to an image taken 1 minute earlier (top left), the coordinates of the oscillating loop show deviations from a semi-circular geometry (bottom left), the loop amplitude measured in perpendicular direction shows also a superimposed trend of centroid motion (top right), and the oscillatory component exhibits strong damping (bottom right) [from Aschwanden *et al.* 2002].

damping, while the slow-mode MHD oscillations seem to be damped by radiative cooling.

Although the young new field of coronal seismology confirmed the theoretically expected MHD modes, there are still a number of significant problems to be worked on, such as the nature of the excitation mechanism, the detailed 3D modeling of asymmetrically excited modes, and the physical nature of the damping mechanism. Alfvénic waves seem also to be excited in the outflows of reconnection regions as reported in some flares. In principle, observations of fast MHD kink-mode oscillations allow us to measure the magnetic field in the solar corona directly, but an accurate determination requires also measurements of the density contrast inside and outside of the loops. One MHD oscillation mode that has not yet been successfully detected is the torsional mode. Detailed 3D modeling of loop oscillations have also to consider the effects of loop curvature, gravitational stratification, the loop cross-section geometry, the polarization direction, coupling of modes, higher harmonics, and temperature effects from radiative and conductive cooling. For recent reviews see, e.g., Aschwanden (2004), Nakariakov & Verwichte (2005).

6. The coronal heating problem

The coronal heating problem has been with us since 6 decades, since Bengt Edlén and Walter Grotrian identified the highly ionized Fe IX and Ca XIV lines in the solar spectrum in 1943, which indicated a coronal temperature of ≈ 1 MK that was about 200 times higher than the underlying chromosphere. Such a hot corona can obviously not be generated by thermal conduction, but requires a specical mechanism that turned out to be difficult to detect directly. Today, we have a bifurcation of two mechanisms that seem to be responsible for heating of the solar corona: (1) a *basal heating mechanism* that is most likely related to small-scale reconnection processes in the transition region, which fills coronal loops in active regions and in the quiet Sun, and (2) an *extended corona heating mechanism* that is most likely generated by ion-cyclotron heating of Alfvén waves, which heat the extended corona and solar wind in a typical distance of $\approx$ 2–5 solar radii.

Recent observations show no evidence for local (*in-situ*) heating in the solar corona in active regions and in the quiet Sun, but rather for a basal heating mechanism that operates below the corona in the transition region and upper chromosphere, with subsequent *chromospheric evaporation* as known in flares. New observational evidence for this scenario comes from (1) the temperature evolution of coronal loops, (2) the over-density of hot coronal loops, (3) upflows in coronal loops, (4) the Dopplershift in coronal loops, (5) upward propagating waves, (6) the energy balance in coronal loops, (7) the magnetic complexity in the transition region, (8) the altitude of nanoflares and microflares, (9) the cross-section of elementary loops, as well as from (10) 3D MHD simulations of coronal heating (such as by Gudiksen & Nordlund 2005). The phrase *coronal heating problem* is therefore a paradoxical misnomer and should rather be addressed as *chromospheric heating problem* and *coronal loop filling process*. This paradigm shift substantially reduces the number of relevant theoretical models for coronal heating in active regions and the quiet Sun (Aschwanden 2007).

In contrast, the heating of coronal holes and the solar wind seems to be accomplished by a different mechanism. SoHO/UVCS has revealed surprisingly large temperatures, outflow speeds, and velocity distribution anisotropies for positive ions in coronal holes. The role of Alfvén waves (their generation, propagation, and reflections) becomes more important on larger spatial scales (since Alfvén waves have a long dissipation length of several solar radii). Wave-particle interactions, such as ion-cyclotron resonance, are considered now as the principal mechanism for heating of coronal holes, and ultimately driving the fast solar wind (Hollweg 2006; Cranmer 2002, 2004). The current understanding is that the solar wind is mainly driven by the pressure of hot protons, so the heating in coronal holes goes more into protons than electrons, because it is conveyed by the ion-cyclotron resonance rather than by currents, which is different from the DC heating models generally applied in the lower corona (basal coronal heating).

7. Self-organized criticality in solar flares

Self-organized criticality is universally manifested by powerlaw distributions of system size parameters, measured on spatial, temporal, or energy scales. Powerlaws are the statistical distributions that result from nonlinear processes, while exponential (or Poisson) distributions are the characteristics of random processes with linear scaling.

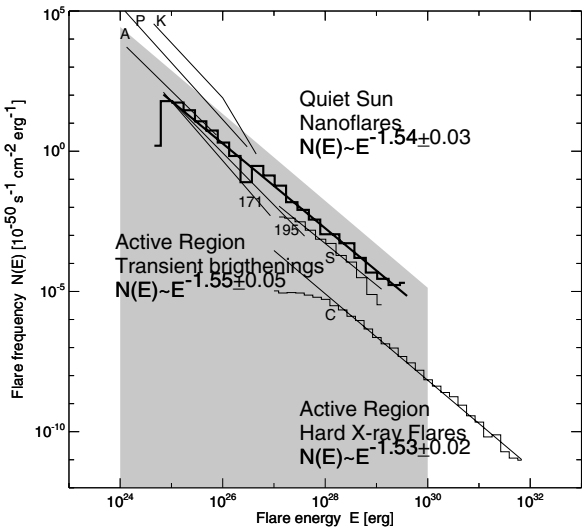

Figure 6. Compilation of frequency distributions of flare energies in the nanoflare range in EUV, active region transient brightenings in soft X-rays and hard X-ray flares. The grey area marks the required energy for coronal heating, which is about a factor of 3 higher than the observed radiated energy.

The principle of self-organized criticality, known from sandpiles, snow avalanches, and earthquakes, has been first applied to solar flares by Lu & Hamilton (1991). Today, the powerlaw found first for large flares, has been extended to microflares (in hard X-rays), active region transient brightenings (in soft X-rays), to nanoflares (in EUV), covering some 8 decades in energy ($\approx 10^{24} - 10^{32}$ erg) (Fig. 6). A crucial question is whether the power law slope at low energies is steeper than the critical value of 2, which would imply that coronal heating is dominantly accomplished by nanoflares and picoflares at the low end of the distribution. At large energies, flares seem to obey a slope of ≈ 1.5, so the total amount of dissipated energy in the solar corona is dominated by the largest giant flares. At the low end, powerlaw slopes for the smallest detected EUV flares have been reported in a range of ≈ 1.6 up to 2.6, but the steeper slopes seem to be biased by incomplete temperature coverage, as well as by unrealistic geometric models that do not include the proper fractal scaling of flare volumes (Aschwanden & Parnell 2002). Nevertheless, also stellar flares seem to show a range of slopes from ≈ 1.5 to ≈ 2.5 (Audard *et al.* 2000), which are not yet properly understood.

8. Magnetic reconnection processes

Although everybody agrees that magnetic reconnection processes are the principal drivers of all eruptive phenomena on the Sun, such as eruptive filaments and prominences, flares, and coronal mass ejections (CME), the detailed magnetic topologies remain subject of intense investigations and may substantially differ from what we can observe *in situ* in the Earth's magnetosphere. The main observational handicap is the lack of illumination and insufficient spatial resolution to map out the magnetic pre-reconnection configuration, while the post-reconnection configuration is usually

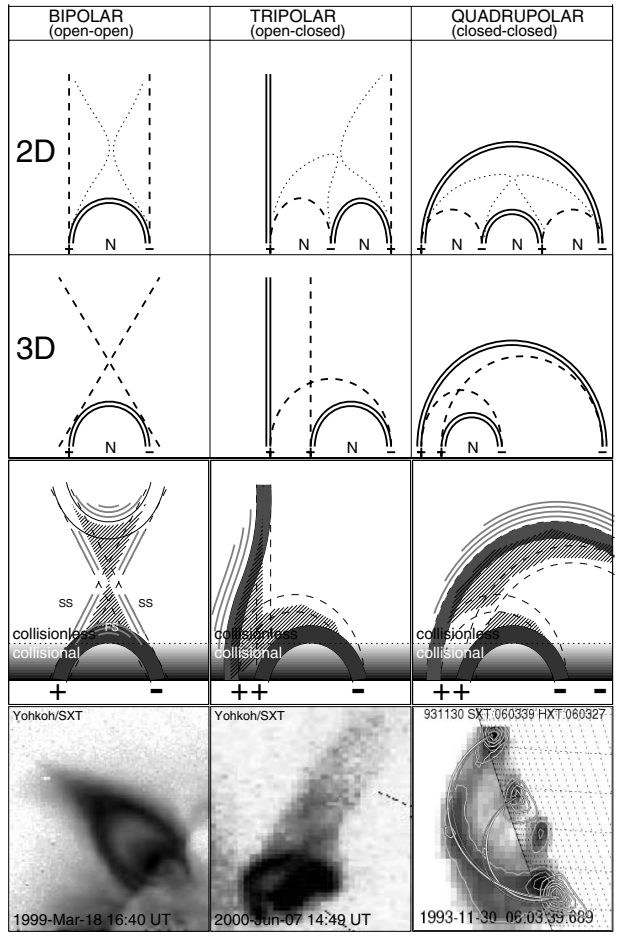

Figure 7. The topology of magnetic reconnection regions is classified into three classes: bipolar or open-open (left column), tripolar or open-closed (middle column), and quadrupolar or closed-closed field line reconnection (right column). The 2D versions are shown in the top row, with the pre-reconnection field lines marked with dashed lines, during reconnection with dotted lines, and post-reconnection field lines with double solid linestyle. The 3D versions are indicated in the second row, where the pre-reconnection field lines are not coplanar, but located behind each other. The third row indicates the acceleration regions (hatched), the relative densities (grey scale), and upward/sideward directed shocks (grey lines). The bottom row shows flare observations from Yohkoh/SXT that correspond to the three different reconnection topologies.

prominently illuminated in soft X-rays and EUV from the chromospherically evaporated hot plasma that fills the post-flare loop system. Therefore, we have to reconstruct the pre-reconnection configuration from topological constraints. The simplest basic configurations can be classified as bipolar, tripolar, and quadrupolar configurations (Fig. 7), which can be approximated by 2D models, or more realistically, with 3D models (Fig. 7, top two rows). Bipolar flares produce also ejecta and Masuda-type above-the-loop-top hard X-ray sources; tripolar flares produce also linear soft X-ray jets; and quadrupolar flares have a stricter confinement of the flare plasma and

might even have no access to open field lines, and thus might lack radio emission from escaping electron beams (i.e., type III bursts). In the meantime we found many more flare by-products that allow us to study quantitatively the process of magnetic reconnection, such as: reconnection inflows detected in EUV, reconnection outflows detected in EUV, footpoint motion and the magnetic field in the flare ribbons that allow us to quantify the evolution of the reconnection rate, high-temperature ridges detected in soft X-rays that mark slow shocks and fast-mode standing shocks predicted by the Petschek reconnection model, and bi-directional electron beams detected in radio and hard X-rays that reveal the symmetry of X-points. More complex scenarios in terms of 3D reconnection have also been inferred from observations, indicating intriguing hints of fan, dome, or spine reconnection.

But there still remain a number of open issues on magnetic reconnection in solar flares:

- the initial configuration and driver (unstable filament or prominence, photospheric flux emergence, converging flows, or shear flows);
- the origin of anomalous resistivity in current sheets and the observed intermittent time structures, which seem to indicate a bursty reconnection mode rather than steady Sweet-Parker or Petschek type reconnection;
- the frequent lack of and low value of inflow velocities observed so far;
- the rare detection of outflows and their dynamic nature, which sometimes is observed to produce oscillatory waves;
- the open-field component at the onset of reconnection that is essential to produce the observed type III bursts;
- the electron number problem between the available coronal flare volume and the hard X-ray producing energetic particles, as well as the high asymmetry in the number of upward and downward accelerated particles. For recent textbooks that deal with magnetic reconnection in solar flares see, e.g., Priest & Forbes (2000); Tajima & Shibata (2002); Aschwanden (2004).

9. Particle acceleration processes

There are three main categories of particle acceleration processes that are thought to play an important role in solar flares and CMEs:

- electric DC-field acceleration,
- stochastic acceleration, and
- shock acceleration (for reviews see, e.g., Miller *et al.* 1997; Aschwanden 2004).

We have realistic scenarios for all three mechanisms and believe that they all can operate in solar flare configurations. The electromagnetic fields near magnetic X-points can accelerate particles in current sheets, wave turbulence provides a suitable environment for stochastic acceleration, and the standing fast-mode shocks in reconnection outflows or the shocks at the fronts and flanks of CMEs are all capable of producing shock acceleration. While there is no shortage of theoretical models, our main problem in understanding which acceleration mechanism is most relevant in solar flares is an observational one. The acceleration mechanism itself is a black box for our instruments, while we can only observe secondary emissions such as hard X-ray bremsstrahlung

once the nonthermal particles slam into the chromosphere, or radio emission once electron beams are formed and propagate into interplanetary space. A key question is also whether solar energetic particles (SEP) observed at 1 AU originate in the coronal flare site or in interplanetary CME shocks. Even detailed energy-dependent timing and spectral studies do not tell us first-hand information about the acceleration mechanism, because the secondary signatures represent a convolved signal of at least 5 different processes: acceleration, injection, propagation, trapping, and energy loss. What is needed to make progress is to measure the 3D magnetic topology in the reconnection region and in shocks, the 3D reconstruction of the electromagnetic fields, the 3D reconstruction of the particle trajectories, and physical modeling of the collisional plasma along their trajectories and energy loss sites – not a small task!

10. Coronal mass ejections

Coronal mass ejections (CMEs) are the last phenomenon in the chain of magnetic instabilities in the solar corona, which start with a filament eruption, generate a flare, and launch a CME (for reviews see, e.g., Alexander 2006; Gopalswamy *et al.* 2005; Zhang & Low 2005; Bothmer & Daglis 2007). CMEs received attention only in the 1980s, when the white-light coronagraphs of SMM showed that CMEs are as frequent as flares. Today, with the coronagraphs LASCO on SoHO and on STEREO, the golden age of CME research started. The chief problems we study are:

- their origin, which is often the same magnetic instability that is responsible to trigger filament eruptions and flares,
- the evolution and propagation of CMEs in interplanetary space, including their spatial topology (twisted flux ropes or half shell-like bow-shocks),
- the dynamic coronal response to a CME launch (coronal dimming, EIT waves, loop oscillations),
- the hydrodynamic modeling of CMEs (in terms of MHD codes that simulate the propagation of a CME shock and its interaction with the ambient solar wind),
- the capability, timing, geometry, and energetics of particle acceleration in CME shocks, and
- the geoeffectivity of CMEs and related space weather effects, a catalog of research problems that becomes bigger every year.

11. Final remarks

This brief sketch of ten outstanding problems in solar physics illustrates what a vibrant research field has been opened up, thanks to the multi-wavelength observations that became available to us by solar-dedicated space missions over the last six decades, such as: Skylab (1973), SMM (1980–1989), Yohkoh (1992–2001), Compton GRO (1991–2000), SoHO (1995-today), TRACE (1998-today), RHESSI (2002-today), and SOXS (2003-today). Now, this golden era is continuing to thrive with new missions such as STEREO (launched in October 2006), HINODE (launched in August 2006), and SDO (to be launched in 2008). We note also that a fundamental transformation took place in our approach to study the Sun over the last six decades: we started from the observationally dominated *solar astronomy* and evolved now into true *solar physics*, where a deeper physical understanding is accomplished by theoretical and numerical modeling.

Acknowledgements

I warmly thank Rajmal Jain and the Organizing Committee of this Jubilee Conference for the generous hospitality at PRL, and Arnab Choudhary for showing me a fascinating tour through Ahmedabad and the Gandhi Ashram in Gujarat. This work is partially supported by NASA contract NAS5-98033 of the RHESSI mission through University of California, Berkeley (subcontract SA2241-26308PG), NASA contract NAS5-38099 for the TRACE mission, and NASA contract N00173-02-C-2035 for the STEREO mission through NRL.

References

Ahmad, Q. R. *et al.* 2002, *Phys. Rev. Lett.*, **89**, 011301.
Alexander, D. 2006, *Space Sci. Rev.*, **123**, 81.
Aschwanden, M. J. *et al.* 1999, *ApJ*, **515**, 842.
Aschwanden, M. J. *et al.* 2000, *ApJ*, **541**, 1059.
Aschwanden, M. J. *et al.* 2001, *ApJ*, **550**, 1036.
Aschwanden, M. J. *et al.* 2002, *Solar Phys.*, **206**, 99.
Aschwanden, M. J., Parnell, C. E. 2002, *ApJ*, **572**, 1048.
Aschwanden, M. J. 2004, *Physics of the Solar Corona*, Springer: New York.
Aschwanden, M. J. 2007, *ApJ*, **661**, 1242.
Audard, M. *et al.* 2000, *ApJ*, **541**, 396.
Bahcall, J. N. 2005, *Physica Scripta*, **T121**, 46.
Bahcall, J. N. *et al.* 2005, *ApJ*, **621**, L85.
Bahcall, J. N. *et al.* 2006, *ApJS*, **165**, 400.
Bellerive, A. 2004, *Internat. J. Modern Physics A*, **19**, 1167.
Bothmer, V., Daglis, I. A. 2007, *Space Weather*, Springer: New York.
Carlsson, M., Stein, R. F. 1997, *ApJ*, **481**, 500.
Charbonneau, P. 2005, *Living Rev. Solar Phys.*, **2**, 2.
Cranmer, S. R. 2002, *Space Sci. Rev.*, **101**, 229.
Cranmer, S. R. 2004, *Proc. SOHO-15: Coronal Heating*, ESA SP-575, 154.
Davis, R. 2003, *Reviews Modern Physics*, **75**, 985.
DePontieu, B. *et al.* 2007, *ApJ*, **655**, 624.
Gilman, P. A. 2000, *Solar Phys.*, **192**, 27.
Gopalswamy, N. *et al.* 2005, *Solar Eruptions and Energetic Particles*, AGU monograph 165, Washington DC.
Gudiksen, B. V., Nordlund, A. 2005, *ApJ*, **618**, 1020 & 1031.
Hollweg, J. V. 2006, *Phil. Trans. R. Soc. A*, **364**, 505.
Lenz, D. D. *et al.* 1999, *ApJ*, **517**, L155.
Lu, E. T., Hamilton, R. J. 1990, *ApJ*, **380**, L89.
Metcalf, T. R. *et al.* 1995, *ApJ*, **439**, 474.
Miller, J. A. *et al.* 1997, *JGR*, **102/A7**, 14631.
Nakariakov, V. M., Verwichte, E. 2005, *Living Rev. Solar Phys.*, **2**, 3.
Priest, E. R., Forbes, T. 2000, *Magnetic Reconnection*, Cambridge Univ. Press.
Rogers, T. M., Glatzmaier, G. A. 2005, *MNRAS*, **364**, 1135.
Rosner, R. *et al.* 1978, *ApJ*, **220**, 643.
Schrijver, C. J. *et al.* 2006, *Solar Phys.*, **235**, 161.
Serio, S. *et al.* 1981, *ApJ*, **243**, 288.
Tajima, T., Shibata, K. 2002, *Plasma Astrophysics*, Perseus Publ., Cambridge.
Warren, H. P., Winebarger, A. R. 2006, *ApJ*, **645**, 711.
Wiegelmann, T., Inhester, B. 2006, *Solar Phys.*, **236**, 25.
Winebarger, A. R., Warren, H. P. 2005, *ApJ*, **626**, 543.
Zhang, M., Low, B. C. 2005, *ARAA*, **43**, 103.